Available online at www.sciencedirect.com
SCIENCE DIRECT®
Journal of Catalysis 224 (2004) 269–277
JOURNAL OF CATALYSIS
www.elsevier.com/locate/jcat

Simulation of the transient CO oxidation over Rh^0/SiO_2 and $Rh^{x+}/Ce_{0.68}Zr_{0.32}O_2$ catalysts

Isabelle Manuel,[a,b] Jérôme Chaubet,[a] Cyril Thomas,[a] Hervé Colas,[b] Nils Matthess,[b] and Gérald Djéga-Mariadassou [a,*]

[a] *Laboratoire de Réactivité de Surface UMR CNRS 7609, Université Pierre et Marie Curie, 4 Place Jussieu, Case 178, 75252 Paris cedex 05, France*
[b] *PSA Peugeot–Citroën, 18 Rue des Fauvelles, 92000 La Garenne-Colombe, France*

Received 3 December 2003; revised 3 March 2004; accepted 8 March 2004

Available online 16 April 2004

Abstract

The simulation of temperature transient CO oxidation by molecular oxygen was performed over well-defined catalytic centers (zero-valent (Rh^0) or oxidized (Rh^{x+})). Over both sites, a reliable estimation of CO light-off temperatures could be achieved. For this purpose, detailed kinetic rate equations were established from the proposed catalytic sequences of elementary steps. Over Rh^0, the detailed rate equation, approximated to a simplified rate equation which is very close to the global power-rate equation, allowed for a good fitting of the transient CO oxidation up to 60% conversion of CO. Over Rh^{x+}, the preexponential factors and the activation energies of the kinetically significant elementary steps were determined. The simulation of transient CO oxidation with the detailed rate equation allowed for a much better fit of the experimental data (up to 60% conversion) than that of the global power-rate equation (up to 10%). Rh^{x+} provides an excellent example of the superiority of the detailed kinetic rate equation over that of the global power rate, the evidence of which could not be revealed over Rh^0. Finally, for Rh^{x+}, the nature of the kinetically significant elementary steps and the limits of these kinetics are discussed on the basis of the estimated preexponential factors.

Keywords: Kinetics; CO oxidation; Global and detailed rate equations; Simulation; Temperature of light-off; Catalytic sequence; Zero-valent rhodium; Oxidized rhodium; Rate constant; Ceria–zirconia

1. Introduction

CO catalytic oxidation has been studied extensively over noble metal-based materials in the last couple of decades [1–7, and references therein]. Although Ertl depicted the mechanism of this reaction as basically rather simple [4], he emphasized that the catalytic oxidation of CO by molecular oxygen could reveal much greater complexity at a molecular level. The rather complex kinetics of CO oxidation [4–6] as well as the well-established importance of this chemical reaction in three-way catalysis for environmental concern [8–10] sustain strong interest in this reaction [11–15]. It is, indeed, of the utmost importance to improve the effectiveness of the catalytic converters in CO removal in order to meet more stringent emission standards in the future [16].

For a gasoline engine, the selection of the most suitable three-way catalysts (TWC) can be achieved by determining the temperature of light-off (T_{lo} corresponding to the temperature at which 50% conversion of a given compound is completed) of pollutants (CO, NO, unburned hydrocarbons). For this purpose, *a simulation of the transient CO oxidation* over commercial catalysts is *one* of the means of selecting and evaluating the most suitable materials [13,14]. This simulation process requires *a rate equation* taking into account the *nature* and *density* of active sites, as well as the *significant rate constants and activation energies* of the catalytic process. Consequently, kinetics of the reaction and transient experiments, at the laboratory scale, must be performed to establish *the best rate equation* for simulating the reaction within the broader range of conversion of CO.

Despite extensive work performed on the kinetics of catalytic CO oxidation, Ertl [4] stressed that *a global power-rate law* was generally unable to describe the full kinetic process under various operating conditions (for illustration

* Corresponding author. Fax: +33 1 44 27 60 33.
E-mail address: djega@ccr.jussieu.fr (G. Djéga-Mariadassou).

0021-9517/$ – see front matter
doi:10.1016/j.jcat.2004.03.011

of this statement, refer to Fig. 4 of the present work). He stresses, in particular, that over a palladium catalyst the global-rate law changes with temperature, the CO adsorption step being either *near* equilibrium at low temperature or *far* equilibrium at high temperature [4]. Thus, a *detailed* rate equation, based upon a sequence of elementary steps, must be established to overcome the rather limited interest of the global power-law equation in describing the kinetics of a given reaction. If the global kinetics does not change with temperature or conversion, such a detailed rate equation should fit the experimental data as it takes into account the evolution of the reaction orders with respect to the reactants.

In addition, most studies have considered only zero-valent noble metal atom, to describe the kinetics of CO catalytic oxidation [17–20]. Under similar experimental conditions, a general agreement has been reported for the reaction orders with respect to reactants and the activation energy of the reaction over either rhodium single crystals [17] or silica- and alumina-supported rhodium catalysts [18–20]. On the other hand, it must be emphasized that ceria always enters the composition of three-way catalyst supports because of its well-known beneficial properties on three-way catalytic reactions [21,22]. Comparable studies performed over catalysts containing ceria have shown, however, marked discrepancies concerning the kinetic parameters of the catalytic oxidation of CO [20,23,24].

The promotional effect of ceria on the catalytic oxidation of CO has been ascribed either to the occurrence of an additional CO oxidation mechanism, involving oxygen species at the interface of rhodium particles [13,14,23,24], or to a catalytic site different from that of the usual zero-valent species [20], i.e., oxidized catalytic species. Hecker and Bell [25] have also suggested such oxidized rhodium species to explain the higher CO–NO turnover rate observed over a preoxidized silica-supported rhodium catalyst in comparison to that found over a prereduced catalyst. More recently, the presence of noble metal-oxidized species has been reported by our group [26–28] and by Hedge and co-workers [29,30] over ceria-promoted catalysts. It must be emphasized that the presence of such a species was suggested in the case of industrial catalysts [28] which is consistent with results reported by Marin and co-workers [13,14]. These authors were unable to achieve the modeling of transient CO oxidation kinetics without including the aforementioned additional mechanism [23,24].

Finally, our group has reported very recently a *kinetic evidence* of the presence of Rh^{x+} surface *cations* over a ceria-promoted catalyst [15]. The CO oxidation kinetic study performed over well-defined catalytic sites, i.e., either zero-valent or oxidized rhodium species, allowed us to demonstrate that the turnover rate of the oxidation of CO by molecular oxygen of the zero-valent rhodium catalytic site was 25 times lower than that of the oxidized one at a temperature of 428 K. This study has, thus, allowed us to reconcile the two main assumptions reported in the literature in explaining the promotional effect of ceria on the catalytic oxidation of CO. Moreover, two different catalytic cycles, which could possibly explain the turnover rate differences found between the two catalytic species, were proposed. These catalytic cycles stressed that at least three zero-valent catalytic sites in close proximity were needed to complete the CO oxidation process, whereas only one was required in the case of the rhodium cation. These catalytic cycles might also explain the observed competitive adsorption of CO and O_2 over the same catalytic sites, as indicated by the -1 reaction order with respect to CO found over the zero-valent catalytic centers, and the *noncompetitive* adsorption of the reactants over the oxidized catalytic site. In the latter case, the catalytic cycle is comparable to those described for "homogeneous" catalysis, and the reaction occurs in the coordinative sphere of the rhodium cation.

The aim of this work is to bring additional insight on the kinetics of CO oxidation by molecular oxygen over the two different kinds of rhodium catalytic sites, i.e., either zero-valent or oxidized catalytic centers. The detailed rate equations are, thus, established according to the catalytic sequences proposed consistently with the determined experimental reaction orders with respect to the reactants [15]. Kinetically significant rate constants, activation energies, and preexponential factors of the Arrhenius equation are estimated in the case of the $Rh^{x+}/Ce_{0.68}Zr_{0.32}O_2$ catalyst. The simulation of the transient oxidation of CO over both catalytic sites, based upon previous detailed rate equations, is then presented. Finally, we shall discuss the limitation of kinetics in order to ascertain the nature of the kinetically significant elementary step.

2. Experimental

The silica (Degussa, Aerosil 50)-supported rhodium catalyst (0.66 wt% Rh) was prepared by incipient wetness impregnation of the support by an aqueous solution of $RhCl_3$, 3 H_2O (Johnson Matthey). The ceria–zirconia (Rhodia, $Ce_{0.68}Zr_{0.32}O_2$)-supported rhodium catalyst (0.29 wt% Rh) was prepared by anionic exchange from an acidic solution of $RhCl_3$, 3 H_2O with the support [26]. After drying in air at room temperature, the materials were dried at 393 K for 3 h. Finally, the catalysts were crushed and sieved to the desired particle size (0.125–0.200 mm). A thorough description of the catalytic materials is shown in Table 1.

The exposed zero-valent rhodium atoms of both catalysts were titrated through a benzene hydrogenation reaction [28], and the results from our previous work [15] are reported in Table 1. This model reaction led to the conclusion that the Rh/SiO_2 material presented only zero-valent rhodium catalytic sites (about 97% of metal exposed), whereas the $Rh/Ce_{0.68}Zr_{0.32}O_2$ catalyst contained only rhodium cations [15], in agreement with previous work [26]. In this latter work, it was shown that the amount of desorbed NO, for NO adsorption–desorption measurements over $Rh/CeZrO_2$ catalysts with various Rh contents, was twice that of the total Rh

Table 1
Properties of the investigated catalysts

	Catalysts	
	Rh^0/SiO_2	$Rh^{x+}/Ce_{0.68}Zr_{0.32}O_2$
Weight sample (g)	0.101	0.200
Rh content (wt%)	0.29	0.66
d_p (mm)	0.125–0.200	0.125–0.200
ρ_p (g L^{-1})	540	1240
PME as Rh^0 (%)	97	0
PME as Rh^{x+} (%)	0	100
L (mol g_{cat}^{-1})	28.25×10^{-6}	62.38×10^{-6}

d_p is the pellet diameter, ρ_p is the pellet density, PME as Rh^0 is the rhodium percentage of metal exposed as Rh^0 determined by benzene hydrogenation reaction [28], PME as Rh^{x+} (%) is the rhodium percentage of metal exposed as Rh^{x+} in agreement with previous published results [26], L is the specific concentration of surface Rh sites.

content, suggesting the formation of Rh dinitrosyl species and that 100% Rh was exposed as Rh cations [26].

Before runs, the catalyst samples were submitted to a temperature-programmed pretreatment from 298 to 773 K (3 K min^{-1}). The temperature was then kept constant at 773 K for 2 h. Silica– and ceria–zirconia-supported catalysts were submitted to a pretreatment under either pure hydrogen (Air Liquide, 100 cm^3_{NTP} min^{-1}) or a CO–NO–O_2 stoichiometric mixture in helium (1.50–0.20–0.65%, hour space velocity = 100,000 h^{-1}) [26], respectively. After being pretreated, the catalysts were flushed at 773 K for 15 min under helium (230 cm^3_{NTP} min^{-1}), and the catalyst temperature was decreased to 298 K. Before carrying out kinetic measurements, two subsequent and reproducible CO–O_2 (0.4–0.2% in He, 230 cm^3_{NTP} min^{-1} total flow rate) temperature-programmed reactions were carried out from 298 to 773 K with a heating rate of 3 K min^{-1} to ensure the reliability of the activation procedure.

The kinetic study was conducted in a U-type quartz dynamic differential microreactor (8 mm internal diameter). Given the high HSV, the reactor section and the fairly low volume of catalyst, a well-mixed gas mixture in contact with the catalyst was created. The composition of the reacting gas mixture may, thus, be considered as identical to that analyzed at the outlet of the reactor which behaves as a continuous stirred tank reactor (CSTR) [31]. The synthetic gas mixture was fed from independent mass-flow controllers (Brooks 5850). The reactor outflow was analyzed using both a CO infrared detector (Maihak, Finor F) and a gas chromatograph (HP 5890) equipped with a two-packed-column system (Porapak Q and Gas chrom MP-1) and a thermal conductivity detector.

As CO oxidation is strongly exothermic, external and internal diffusion limitations were verified under transient experimental conditions. Koros–Nowak criteria were used [35]. External diffusion was first investigated by varying the total flow rate (F_{TOT}, L s^{-1}), while maintaining a constant contact time ($t = V/F_{TOT}$ (s), V being the catalyst volume (L)), by adjusting the $Rh^{x+}/Ce_{0.68}Zr_{0.32}O_2$ catalyst loading (Fig. 1).

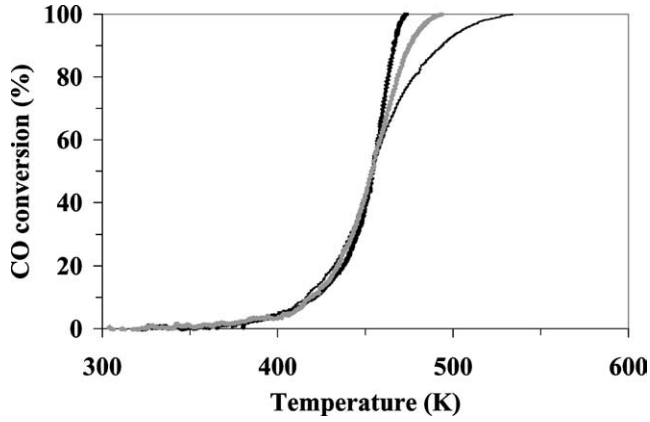

Fig. 1. CO–O_2 temperature-programmed reactions (3 K min^{-1}, 0.4–0.2% in He) over cation rhodium catalytic sites ($Rh^{x+}/Ce_{0.68}Zr_{0.32}O_2$): (—) 0.4 g of catalyst and $F_{TOT} = 400$ mL min^{-1}, (—) 0.2 g of catalyst and $F_{TOT} = 200$ mL min^{-1}, (—) 0.1 g of catalyst and $F_{TOT} = 100$ mL min^{-1}.

These experiments show that external limitations only occurred at CO conversions higher than 60%. Internal diffusion was also investigated over $Rh^{x+}/Ce_{0.68}Zr_{0.32}O_2$ by varying the grain size (0.125–0.200 or 0.200–0.315 mm) for a given contact time. As in the case of external diffusion, a deviation could be observed at CO conversions higher than 60% (not shown). Finally, it can be concluded that both external and internal diffusions occurred for the CO–O_2 reaction for CO conversions higher than 60%.

The global kinetic parameters reported here were obtained under steady-state conditions (Table 2), while operating the reactor isothermally and as closely to differential reactor as possible by limiting the conversion to less than 10%.

CO oxidation transient experiments were simulated with the help of the Microsoft Excel 97 software using a standard PC computer. For the global-rate equation determined over Rh^0/SiO_2 [15], the simulation was performed according to the following method: The reaction rate was first estimated at a given temperature (T) by means of the corresponding rate equation,

$$r_{Rh^0,global} = k_{Rh^0,global}[CO]_i^{-1}[O_2]_i^{+1}, \quad (1)$$

with $k_{Rh^0,global} = A\exp(-E_a/(RT))$, $k_{Rh^0,global}$, $[CO]_i$, $[O_2]_i$, A, and E_a being the experimental kinetic constant (mol L^{-1} s^{-1}), the initial CO and O_2 gas-phase concentrations (mol L^{-1}), the preexponential factor (mol L^{-1} s^{-1}), and the activation energy (J mol^{-1}), respectively.

The reactor mole balance of a CSTR was then considered,

$$F_{TOT}[CO]_T = F_{TOT}[CO]_i - r_{Rh^0,global}V, \quad (2)$$

with F_{TOT}, $[CO]_T$, and V being the total flow rate (L s^{-1}), the CO gas-phase concentration at a temperature T (mol L^{-1}), and the reactor volume (L), respectively. In the case of a CSTR, the reactor volume corresponds to the catalyst volume. By dividing Eq. (2) by F_{TOT}, the CO gas-phase concentration can be calculated at a given temperature ($[CO]_T$):

$$[CO]_T = [CO]_i - r_{Rh^0,global}t. \quad (3)$$

Table 2
Reaction conditions used for the CO–O_2 studies

	Experiment	[CO] (%)	[O_2] (%)	Total flow rate ($m(L_{NTP})\,min^{-1}$)	T (K)	
Rh^0/SiO_2	CO reaction order	0.22–0.70	0.20	170–400	428	[15]
	O_2 reaction order	0.40	0.13–0.60	170–400	428	[15]
	Activation energy	0.40	0.20	230	428–440	[15]
	CO–O_2 light-off	0.40	0.20	230	298–773	This study
$Rh^{x+}/Ce_{0.68}Zr_{0.32}O_2$	CO reaction order	0.22–0.70	0.20	170–400	403	[15]
	O_2 reaction order	0.40	0.16–0.60	170–400	403	[15]
	Activation energy	0.40	0.20	230	403–423	[15]
	CO–O_2 light-off	0.40	0.20	230	298–773	This study
	Elementary steps[a]	0.40	0.18–0.25	170–400	398–413	This study

[a] These reaction conditions refer to the determination of k_5 and k_6 or k_{10} and the corresponding preexponential factors and activation energies, reported in Table 3, of elementary steps from Fig. 5.

Finally, CO conversion at a given temperature ($CO_{conv.,T}$) was calculated as

$$CO_{conv.,T}\ (\%) = \frac{[CO]_i - [CO]_T}{[CO]_i} \times 100. \quad (4)$$

3. Results and discussion

3.1. Kinetics and simulation of the transient CO oxidation experiment over zero-valent rhodium catalytic centers (Rh^0/SiO_2)

As already noted in the Introduction, kinetics of CO oxidation over zero-valent sites has been addressed by many authors [1,5,6,13,14,32–34]. It appeared relevant to briefly recall how the rate equation may be established, in order to provide the basis for a comparison with that of the rhodium cation site (Section 3.2), and to indicate the high degree of reliability of the simulation of CO oxidation using this rate equation.

3.1.1. Overall reaction and global power-rate equation

The overall reaction, $2CO + O_2 = 2CO_2$, will be considered. For a conversion lower than 10%, the global power-rate equation [5] has already been published by many different groups [4,6,13,15,17–20,32,33]:

$$r_{Rh^0,global} = k_{Rh^0,global}[CO]^{-1}[O_2]^{+1}. \quad (5)$$

From our previous work [15], the global activation energy ($E_{a,Rh^0,global}$) and the preexponential factor ($A_{Rh^0,global}$) were estimated to 131 kJ mol^{-1} and 2.7×10^{12} mol L^{-1} s^{-1}, respectively.

3.1.2. Sequence of elementary steps and detailed rate equation

To summarize, the well-established [6,13,18,34,35] catalytic sequence of elementary steps for CO oxidation over zero-valent noble metal species, in agreement with our already published catalytic cycle [15], is shown in Fig. 2.

Step no.	Elementary Step	σ_i	
[1]	$CO + * \rightleftharpoons CO*$	2	K_1
[2]	$O_2 + * \rightsquigarrow O_2*$	1	k_2
[3]	$O_2* + * \longrightarrow 2\,O*$	1	
[4]	$CO* + O* \longrightarrow CO_2 + 2*$	2	
	$2\,CO + O_2 = 2\,CO_2$	overall reaction	

Fig. 2. CO oxidation catalytic sequence over zero-valent rhodium atoms, * and σ_i being a zero-valent rhodium atom and the stoichiometric numbers expressing the number of times each elementary reaction has to proceed for the corresponding closed sequence to turn over once, respectively.

Symbols and definitions were recalled in a recent paper [34]. Symbols for elementary steps in a sequence are: "one-way" or irreversible ($\longrightarrow$), "two-way" or reversible, but far equilibrium ($\rightleftharpoons$), or near equilibrium ($\rightleftharpoons$). The symbol ($\rightsquigarrow$) stands for the rate-determining step (rds); σ_i is the stoichiometric number that expresses the number of times each elementary reaction has to proceed for the corresponding closed sequence to turn over once; "*" stands for free Rh^0 active site and adsorbed species M are symbolized by *M. K_i and k_i are equilibrium and rate constants, respectively.

At low temperatures and conversions, taking into account the negative reaction order with respect to CO, *CO is assumed to be the most abundant reactive intermediate (mari [34]). The high CO surface coverage is in agreement with Ertl's data over palladium [4] and it also justifies the molecular adsorption of oxygen in step 2. Let us pay particular attention to this point. In the literature [13,32], justification for molecular adsorption of oxygen is somewhat confusing. This elementary step could, thus, not be included "explicitly" in the catalytic sequence, as reported by Oh et al. [32]. These authors [13,32] justified it on the basis of previous oxygen adsorption work performed over "clean" metallic surfaces [36,37]. Under such experimental conditions, it is not surprising that oxygen dissociates, the probability of finding a pair of adjacent active sites being rather high on a "clean" metallic surface. Under our reacting experimental conditions, *CO being the mari, pairs of free adjacent sites are not abundant, and statistically, oxygen

only finds isolated free sites *. Once *CO has scavenged an *O species adjacent to an O*O species (step 4), step 3 can proceed and oxygen dissociates. Such a catalytic sequence is, thus, in agreement with the first order that was determined with respect to O_2.

The detailed rate equation for this sequence is established following the method recently recalled [34]:

1. The application of the quasi-stationary state approximation (QSSA) leads to

$$r_{Rh^0} = \frac{r_2}{\sigma_2} = k_2[O_2][^*] \quad \text{(rds)}. \tag{6}$$

2. The equilibrium constant (K_1) corresponding to the CO adsorption step 1 is

$$K_1 = \frac{[^*CO]}{[CO][^*]}. \tag{7}$$

3. The balance on the density of active sites, symbolized by L_{Rh^0}, *CO being the mari, is

$$L_{Rh^0} = [^*] + [^*CO]. \tag{8}$$

From these equations, it is easy to obtain the following rate equation:

$$r_{Rh^0} = \frac{k_2[L_{Rh^0}][O_2]}{1 + K_1[CO]}. \tag{9}$$

If [*CO] is large compared to [*], then K_1 [CO] is much higher than 1, and Eq. (9) simplifies to

$$r_{Rh^0} = \frac{k_2[L_{Rh^0}][O_2]}{K_1[CO]}. \tag{10}$$

From this latter simplified equation, reaction orders with respect to O_2 and CO are, therefore, +1 and −1, respectively, and the experimental orders are verified. Comparison of Eq. (10) with Eq. (5) shows that $(k_2[L_{Rh^0}])/K_1$ is equivalent to the experimental kinetic constant of the global power rate law ($k_{Rh^0,global}$). In this case, it was not possible to determine k_2 and K_1 separately. Let us note that this is not a Langmuir–Hinshelwood equation, and that CO inhibits the reaction.

3.1.3. Simulation of the transient CO oxidation on Rh^0/SiO_2 catalyst

The simulation of the CO light-off experiment was performed according to Eq. (10) with $k_{Rh^0,global} = (k_2[L_{Rh^0}])/K_1$. The values of the preexponential factor and the activation energy are given in Section 3.1.1. Fig. 3 shows that the use of this simplified rate law with experimental global kinetic parameters allows for a reliable simulation of the experimental data up to a conversion of CO of 60%. At higher conversions than 60%, strong deviation would occur between experimental and simulated data. In agreement with Fig. 1, this deviation can be attributed to a change from a kinetically controlled domain to a diffusional-controlled domain. We must note, nonetheless, that even though experimental steady-state measurements were carried out with conversions lower than 10%, the simplified kinetic rate law [Eq. (10)] allows for a reliable estimation of the temperature of light-off of CO.

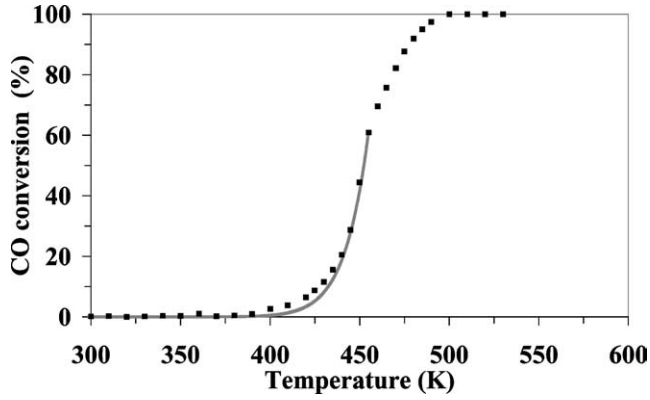

Fig. 3. Experimental (■) and simulated (—) temperature transient CO–O_2 data (3 K min^{-1}, 0.4–0.2% in He, $F_{TOT} = 230$ mL min^{-1}) using a global power-rate kinetic equation ($r_{Rh^0,global} = k_{Rh^0,global}[CO]^{-1}[O_2]^{+1}$, $k_{Rh^0,global} = A_{Rh^0,global} \exp^{(-E_{a,Rh^0,global}/RT)}$) over zero-valent rhodium sites (Rh^0/SiO_2), where $r_{Rh^0,global}$, [CO], [O_2], $k_{Rh^0,global}$, $A_{Rh^0,global}$, and $E_{a,Rh^0,global}$ denote the reaction rate (mol L^{-1} s^{-1}), the gas-phase concentrations of CO and O_2 (mol L^{-1}), the experimental global kinetic constant (mol L^{-1} s^{-1}), the experimental preexponential factor (mol L^{-1} s^{-1}), and the apparent activation energy (J mol^{-1}), respectively. $A_{Rh^0,global} = 2.7 \times 10^{12}$ mol L^{-1} s^{-1}, $E_{a,Rh^0,global} = 131 \times 10^3$ J mol^{-1}.

3.2. Kinetics and simulation of the transient CO oxidation experiment over oxidized rhodium catalytic centers ($Rh^{x+}/Ce_{0.68}Zr_{0.32}O_2$)

The kinetics of CO oxidation over pure oxidized rhodium species has not been reported on up to now by other groups. Beneficial effects of ceria on CO oxidation have, however, been reported by Yu Yao over ceria-promoted rhodium and platinum catalysts [20], and by Bunluesin et al. [23] and Oh and Eickel [24] over ceria-supported rhodium catalysts. Transient modeling of catalytic CO oxidation by Pt/Al_2O_3 and bimetallic $Pt–Rh/CeO_2–Al_2O_3$ catalysts has also been investigated by Marin and co-workers [13,14]. In these studies, it is very likely that the tested catalysts always included a mixture of zero-valent and oxidized catalytic centers such that unambiguous discrimination of the kinetics for the latter catalytic species could not be determined. The kinetic modeling of transient CO oxidation reported by Marin and co-workers [13,14] could not be completed without including a "bifunctionnal path," most likely involving oxidized noble metal catalytic sites to the usual "monofunctionnal path" involved for zero-valent noble metal catalytic centers.

3.2.1. Global power-rate equation

From our previous work [15], results obtained over oxidized rhodium catalytic sites showed striking differences for

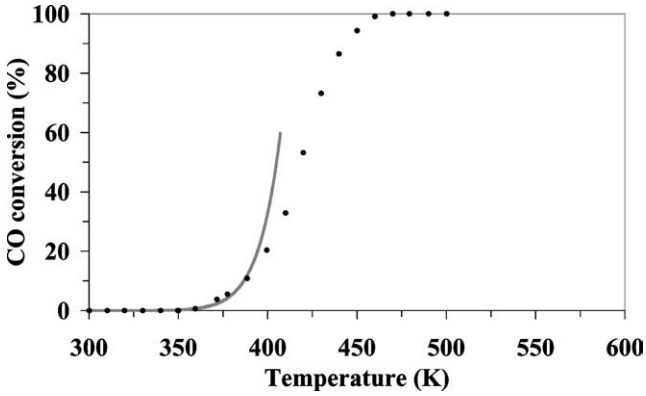

Fig. 4. Experimental (●) and simulated (—) temperature transient CO–O_2 data (3 K min^{-1}, 0.4–0.2% in He, F_{TOT} = 230 mL min^{-1}) using a global power-rate kinetic equation ($r_{Rh^{x+},global} = k_{Rh^{x+},global}[CO]^{+0.4}[O_2]^{+0.1}$, $k_{Rh^{x+},global} = A_{Rh^{x+},global}e^{(-E_{a,Rh^{x+},global}/RT)}$) over cation rhodium sites (Rh^{x+}/$Ce_{0.68}Zr_{0.32}O_2$), where $r_{Rh^{x+},global}$, [CO], [O_2], $k_{Rh^{x+},global}$, $A_{Rh^{x+},global}$, and $E_{a,Rh^{x+},global}$ denote the reaction rate (mol L^{-1} s^{-1}), the gas-phase concentrations of CO and O_2 (mol L^{-1}), the experimental global kinetic constant (mol$^{0.5}$ L$^{-0.5}$ s^{-1}), the experimental preexponential factor (mol$^{0.5}$ L$^{-0.5}$ s^{-1}), and the apparent activation energy (J mol^{-1}), respectively. $A_{Rh^{x+},global} = 5.8 \times 10^{13}$ mol$^{0.5}$ L$^{-0.5}$ s^{-1}, $E_{a,Rh^{x+},global} = 114 \times 10^3$ J mol^{-1}.

the experimental kinetic parameters compared to those of zero-valent rhodium sites. Over oxidized rhodium species, reaction orders of +0.4 and +0.1 were, indeed, estimated with respect to CO and O_2, respectively, as compared to those obtained for zero-valent ones (−1 and +1 reaction orders with respect to CO and O_2, respectively). These reaction orders, nonetheless, fell within the quite confusing range of values reported for ceria-promoted catalysts [20,23,24]. In these earlier studies, the reaction orders most probably may be accounted for by the undefined mixtures of both zero-valent and oxidized rhodium catalytic species.

The experimental global power rate has been found to be as

$$r_{Rh^{x+},global} = k_{Rh^{x+},global}[CO]^{+0.4}[O_2]^{+0.1}. \quad (11)$$

From our previous work [15], the global activation energy ($E_{a,Rh^{x+},global}$) and the preexponential factor ($A_{Rh^{x+},global}$) were estimated to be 117 kJ mol^{-1} and 5.8×10^{13} mol$^{0.5}$ L$^{-0.5}$ s^{-1}, respectively.

3.2.2. Simulation of the transient CO oxidation on $Rh^{x+}/Ce_{0.68}Zr_{0.32}$ catalyst according to a global power-rate law

The simulation of the CO light-off experiment, by means of the global power-law equation, is shown in Fig. 4. A satisfactory correlation can be observed for conversions lower than 10% for which the kinetic measurements were performed. Such a global power-rate law equation does not allow for a reliable simulation of experimental CO light-off data, whereas that determined for the zero-valent rhodium catalytic centers does so (Fig. 3).

Step no.	Elementary Step			Reaction path $\sigma_{L\text{-}H}$	Reaction path $\sigma_{E\text{-}R}$	
[5]	$O_2 + \square^*\square$	⟶	O^*O	1	1	k_5
[6]	$CO + O^*O$	⟶	$CO(O^*O)$	1	0	k_6
[7]	$CO(O^*O)$	⟶	$CO_2 + \square^*O$	1	0	
[8]	$CO + \square^*O$	⟶	$CO(\square^*O)$	1	0	
[9]	$CO(\square^*O)$	⟶	$CO_2 + \square^*\square$	1	0	
[10]	$CO + O^*O$	⟶	$CO_2 + \square^*O$	0	1	k_{10}
[11]	$CO + \square^*O$	⟶	$CO_2 + \square^*\square$	0	1	
	$2\,CO + O_2$	=	$2\,CO_2$	overall reaction		

Fig. 5. CO oxidation catalytic sequence over oxidized rhodium atoms, $\square^*\square$ and σ_i being a rhodium cation surrounded by two oxygen vacancies and the stoichiometric numbers expressing the number of times each elementary reaction has to proceed for the corresponding closed sequence to turn over once, respectively. $\sigma_{L\text{–}H}$ and $\sigma_{E\text{–}R}$ are related to the paths comprising Langmuir–Hinshelwood and Eley–Rideal elementary steps, respectively.

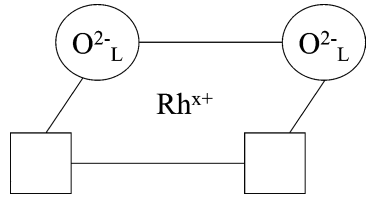

Fig. 6. Model of the complex Rh^{x+} active site, stabilized on the $Ce_{0.68}Zr_{0.32}O_2$ surface. Lattice oxygen from the ceria and oxygen vacancy are referred to as O_L^{2-} and □, respectively.

3.2.3. Sequences of elementary steps and detailed rate equation

The two sequences of elementary steps that can be considered over the rhodium cation catalytic center are shown in Fig. 5. The present sequences consider a rhodium cation, stabilized at the surface of the ceria–zirconia support and surrounded by two oxygen vacancies, as a unique complex active site which is shown in Fig. 6 (denoted $\square^*\square$ in the catalytic sequences shown in Fig. 5). This model of a complex active site is quite different from those assumed by Marin and co-workers [13,14] who considered Pt^0 and Rh^0 as a *first* kind of site, and a *second* kind of site for the adsorption of oxygen on top of the ceria lattice or oxygen vacancies at the surface of the ceria lattice. Let us note that it is difficult to write a *unique* catalytic cycle with *two* different kinds of catalytic sites, unless one of them transforms to the other, as in the case of catalytic hydrogenation over a Wilkinson complex [35]. These catalytic sequences differ from each other in the nature of the elementary step involved in the formation of CO_2. In the first path ($\sigma_{L\text{–}H}$), CO_2 formation occurs through a Langmuir–Hinshelwood surface reaction, whereas in the second path ($\sigma_{E\text{–}R}$), its formation occurs through an Eley–Rideal step.

The former path involves a Langmuir–Hinshelwood surface reaction between adsorbed species (step 7) and corresponds to the catalytic cycle previously proposed [15]. The active site depicted in this catalytic sequence can be compared to the ruthenium carbonyl cation used by Goncharov et al. [38] for the gas-phase oxidation of CO.

From this sequence (Fig. 5, σ_{L-H}), step 5 corresponds to the dissociative insertion of oxygen on the active site. CO(O*O) represents two oxygen anions and CO as ligands in the coordinative sphere of the rhodium cation. □*O stands for one oxygen vacancy and one oxygen anion in the complex active site, once the first oxygen anion has been consumed by reaction with the first CO molecule. CO(□*O) represents the second CO insertion in the coordinative sphere of the rhodium cation. In this catalytic sequence, all elementary steps are far equilibrium. To obtain the detailed rate equation, only steps 5 and 6 are kinetically significant [34]. Taking into account the absence of steps near equilibrium, let us apply the general method:

1. The QSSA tells us that the rate of reaction is such that

$$r_{Rh^{x+}} = r_5 = r_6. \tag{12}$$

More particularly, for defining the rate, let us choose

$$r_{Rh^{x+}} = r_5 = k_5[O_2][\square^*\square]. \tag{13}$$

2. The balance on the density of sites, assuming now that the mari is O*O due the well-known high affinity of ceria for oxygen [22], is given by

$$[L_{Rh^{x+}}] = [\square^*\square] + [O^*O]. \tag{14}$$

Eqs. (12) to (14) lead to the following detailed rate expression:

$$r_{Rh^{x+}} = \frac{k_5 k_6[CO][O_2][L_{Rh^{x+}}]}{k_5[O_2] + k_6[CO]}. \tag{15}$$

Let us note that this equation does not correspond to a Langmuir–Hinshelwood mechanism even if it comprises a Langmuir–Hinshelwood surface reaction.

On the other hand, the second path (Fig. 5, σ_{E-R}) involves an Eley–Rideal step (step 10). Nevertheless, it must be emphasized that a detailed rate equation similar to Eq. (15) can be obtained by applying the aforementioned methodology to steps 5 and 10 [Eq. (16)]:

$$r_{Rh^{x+}} = \frac{k_5 k_{10}[CO][O_2][L_{Rh^{x+}}]}{k_5[O_2] + k_{10}[CO]}. \tag{16}$$

Considering the linear transforms of Eq. (15) or (16),

$$\frac{1}{r_{Rh^{x+}}} = \frac{1}{k_6[CO][L_{Rh^{x+}}]} + \frac{1}{k_5[O_2][L_{Rh^{x+}}]}, \tag{17}$$

$$\frac{1}{r_{Rh^{x+}}} = \frac{1}{k_{10}[CO][L_{Rh^{x+}}]} + \frac{1}{k_5[O_2][L_{Rh^{x+}}]}, \tag{18}$$

further kinetic measurements were performed with a *fixed* concentration of CO (0.4%) and various O_2 concentrations ranging from 0.18 to 0.25%. By plotting $1/r_{Rh^{x+}}$ versus $1/[O_2]$, a straight line was obtained. The values of the slope and the ordinate axis intercept allowed the calculation of the rate constants k_5 and k_6 or k_{10} of steps 5 and 6 or 10. The same methodology, applied at various temperatures between 398 and 413 K, led to the determination of the corresponding preexponential factors and activation energies (Table 3).

Table 3
Experimental preexponential factors (A) and activation energies (E_a) of the elementary steps 5 and 6 or 10 of the oxidized rhodium catalytic sequence (Fig. 5)

	A (L mol^{-1} s^{-1})	A (cm^3 s^{-1})	E_a (kJ mol^{-1})
Step 5	1.45×10^{18}	2.41×10^{-3}	123
Step 6 or 10	1.24×10^{7}	2.06×10^{-14}	39

For the sake of comparison with values already reported in the literature, A is given with two units.

3.2.4. Simulation of the transient oxidation of CO over $Rh^{x+}/Ce_{0.68}Zr_{0.32}O_2$

The detailed rate-law equation (15) and the corresponding elementary kinetic parameters (Table 3) were used to simulate the transient oxidation of CO (Fig. 7). It must be emphasized that the correlation between experimental and simulated data is much better than that issued from the global power-rate-law equation (Fig. 4). Indeed, a satisfying simulation is observed up to 60% conversion of CO, whereas the simulation could only be achieved up to 15% conversion of CO for the global power-law equation (Fig. 4), the conversion range in which the kinetic measurements were performed. This correlation was obtained with very slightly adjusted values (within the experimental uncertainties) of the activation energies of the elementary steps used for the simulated data shown in Fig. 7. Note that a better simulation could never be achieved by applying a comparable adjustment in the case of the global power-rate equation [Eq. (10)]. For conversions of CO higher than 60%, the detailed rate law would no longer fit the experimental data, most proba-

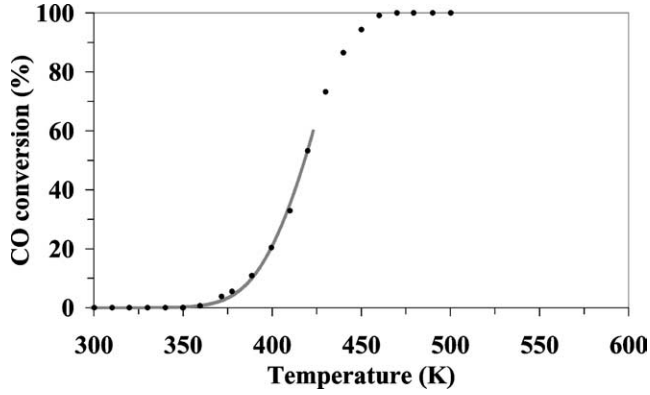

Fig. 7. Experimental (●) and simulated (—) temperature transient CO–O_2 data (3 K min^{-1}, 0.4–0.2% in He, F_{TOT} = 230 mL min^{-1}) using a detailed rate kinetic equation ($r_{Rh^{x+}} = ((k_5 k_6[CO][O_2][L_{Rh^{x+}}])/(k_5[O_2] + k_6[CO])$, $k_i = A_i \exp^{(-E_{a,i}/(RT))}$) over oxidized rhodium sites ($Rh^{x+}/Ce_{0.68}Zr_{0.32}O_2$), where $r_{Rh^{x+}}$, [CO], [O_2], $[L_{Rh^{x+}}]$, k_i, A_i, and $E_{a,i}$ denote the reaction rate (mol L^{-1} s^{-1}), the gas-phase concentrations of CO and O_2 (mol L^{-1}), the number of oxidized rhodium catalytic sites (mol L^{-1}), the kinetic constant of the elementary step i (L mol^{-1} s^{-1}), the preexponential factor of the elementary step i (L mol^{-1} s^{-1}), and the activation energy of the elementary step i (J mol^{-1}), respectively. $[L_{Rh^{x+}}] = 3.5 \times 10^{-2}$ mol L^{-1}, $A_5 = 1.45 \times 10^{18}$ L mol^{-1} s^{-1}, $E_{a,5} = 120 \times 10^3$ J mol^{-1}, $A_6 = 1.24 \times 10^7$ L mol^{-1} s^{-1}, and $E_{a,6} = 38 \times 10^3$ J mol^{-1}.

bly because of diffusion limitations. Finally, it is important to note that a reliable estimation of the CO light-off temperature is achieved with the simulation using the detailed rate law [Eq. (15)].

3.3. Comparison of CO transient kinetics of supported Rh^0 and Rh^{x+} catalytic centers

This comparative study of zero-valent and oxidized rhodium catalytic centers raises an interesting kinetic feature. As noted above, in the case of zero-valent catalytic sites, it is clear that the reaction orders with respect to CO and O_2 are valid over a broad range of conversion of CO (Fig. 3, 0–60%) even though they were determined in a narrower range of conversion. On the other hand, over the rhodium cation catalytic sites, it was shown that the reaction orders were valid in a much narrower range of CO conversion (Fig. 4, 0–10%) compared to that of the zero-valent species. In this case, the use of a detailed rate equation was required.

The very low amount of rhodium of commercial catalysts (less than 0.035 wt% related to the monolith which corresponds to less than 0.3 wt% of the wash coat) makes the characterization of the metal by traditional techniques such as transmission electron microscopy, X-ray photoelectron spectroscopy, X-ray diffraction, and extended X-ray absorption fine structure most difficult. Kinetics and catalysis offer a promising tool for providing the evidence of zero-valent and cationic rhodium catalytic sites. Indeed, the comparison of the CO transient oxidation has shown that the kinetic behaviors of these two catalytic centers are quite different (Figs. 3 and 7). These different behaviors are in turn confirmed by the very different detailed rate equations proposed in our work [Eqs. (9) and (15) or (16)], which in both cases have been shown to provide reliable estimations of the CO light-off temperatures.

For both catalytic sites, the turnover rates estimated at 428 K from our previous work [15] are recalled in Table 4. It must be emphasized that the turnover rate determined over zero-valent rhodium sites is in good agreement with that reported by Cant et al. [18] over the same catalyst (Rh/SiO_2). The comparison of the turnover rate found in our previous work with those reported over alumina-supported Rh catalysts [19,32] is more difficult. Over alumina-supported Rh catalysts, the presence of oxidized Rh sites, coexisting with zero-valent ones, cannot be ruled out. Such a possibility has been suggested by Yu Yao [20], the evidence of which has been ascertained by Trautmann and Baerns [39] through CO adsorption followed by DRIFT.

Table 4
Estimated turnover rates of Rh^0 and Rh^{x+} catalytic sites at 428 K

Catalyst sample	Catalytic site	Turnover rate[a] (10^{-4} s^{-1})
Rh/SiO_2	Rh^0	54
$Rh/Ce_{0.68}Zr_{0.32}O_2$	Rh^{x+}	1320

[a] Mol of CO_2 formed per mole of either Rh^0 or Rh^{x+}.

Because of the much higher reactivity of Rh-oxidized sites (Table 4), the much higher turnover rates reported over alumina-supported Rh catalysts [19,32], compared with those determined for silica-supported Rh catalysts [15,18], might be assigned to the presence of Rh-oxidized catalytic sites in the studied catalysts [19,32].

3.4. Limits of the kinetic approach in determining the nature of the significant elementary steps of the Rh^{x+} catalytic sequence

In particular cases, Boudart and Djéga-Mariadassou [35] have already emphasized the potential ambiguity in the nature of the kinetically significant elementary steps leading to the detailed rate equation.

Considering the catalytic sequences proposed over the rhodium cation catalytic site (Fig. 5), the preexponential factor was experimentally estimated to be 2.41×10^{-3} cm^3 s^{-1} for step 5 (Table 3). This factor is quite different from that expected from a dissociative adsorption process reported by Zhdanov et al. [40], Baetzold and Somorjai [41], or Krylov et al. [42]. For this particular elementary process, these authors listed values of the preexponential factor included in the 10^{-10}–10^{-17} cm^3 s^{-1} range. It is worth reporting that these values were estimated over zero-valent noble metals, whereas that estimated in the present work is related to Rh cation sites. This difference might be assigned to the O adatom to noble metal surface atom ratio. In the former case, a ratio of 1 is considered, whereas 1 Rh cation accommodates 2 O adatoms.

In contrast to the preexponential factor estimated for step 5, that estimated for step 6 or 10 (2.06×10^{-14} cm^3 s^{-1}, Table 3) is in good agreement with those reported by Zhdanov et al. [40] and Krylov et al. [42] either for molecular adsorption or for Eley–Rideal elementary steps.

In the case of associative adsorption steps, it is interesting to note that the O adatom to noble metal surface atom ratio is 1 both for zero-valent noble metal and for cation surface catalytic sites, which was not the case for step 5.

It may appear controversial to be unable to discriminate between molecular adsorption and Eley–Rideal elementary steps (Fig. 5). Nevertheless, this last point is much less controversial if one considers the balance of steps 6 and 7 (Fig. 8). Such a balance is nothing but the Eley–Rideal step 10. It becomes rather obvious that *if k_7 is much higher*

Step no.	Elementary Step	$\sigma_{L\text{-}H}$	
[6]	$CO + O^*O \longrightarrow CO(O^*O)$	1	k_6
[7]	$CO(O^*O) \longrightarrow CO_2 + \square^*O$	1	k_7
[10]	$CO + O^*O \longrightarrow CO_2 + \square^*O$		k_{10}

Fig. 8. Limits of the kinetic approach in determining the nature of the significant steps of the Rh^{x+} catalytic sequences (Fig. 5): comparison of step 6 (Langmuir–Hinshelwood reaction path) and the balance of steps 6 and 7 (step 10, Eley–Rideal reaction path). O^*O and $O^*\square$ being a rhodium cation surrounded by two oxygen anions and a rhodium cation surrounded by one oxygen anion and a vacancy, respectively.

than k_6, the CO(O*O) intermediate has a *very short lifetime*, and the reaction is equivalent to an Eley–Rideal process. This interesting kinetic feature, thus, stresses the limits of kinetics as already reported for CO oxidation by Marin and co-workers who were unable to discriminate between a Langmuir–Hinshelwood and an Eley–Rideal step over a supported zero-valent Pt–Rh catalyst [13].

4. Conclusion

The simulation of transient CO oxidation by molecular oxygen of a stoichiometric mixture was performed over supported rhodium catalysts exhibiting either zero-valent (Rh^0) or oxidized (Rh^{x+}) catalytic centers. For this purpose, the detailed kinetic rate equations were established from the proposed catalytic sequences of elementary steps. For the Rh^0 catalytic sites, it was shown that the detailed rate equation, which could be approximated to a simplified rate equation very close to the global power-rate equation, allowed for a good fitting of the temperature transient CO oxidation up to 60% conversion of CO. On the other hand, over the Rh^{x+} catalytic sites, the temperature transient CO oxidation could only be satisfactorily fitted up to 10% conversion with the global power-rate equation. In this latter case, additional kinetic measurements were performed to determine the preexponential factors and the activation energies of the kinetically significant elementary steps. The simulation of the transient CO oxidation based on the detailed rate equation and the associated kinetic parameters of the elementary steps allowed for a much better fit of the experimental data. The conversion of CO could be simulated up to 60%. Over both catalytic sites, a reliable estimation of the temperature of light-off of CO could be achieved. The rhodium cation catalytic center (Rh^{x+}), thus, provides an excellent example of the superiority of the detailed kinetic rate equation over that of the global power rate, the evidence of which could not be revealed over Rh^0 active sites. Finally, in the case of Rh^{x+}, the nature of the kinetically significant elementary steps and the limits of kinetics are discussed on the basis of the estimated preexponential factors.

Acknowledgments

PSA Peugeot–Citroën has provided financial support for this work; the ADEME (Agence de l'Environnement et de la Maîtrise de l'Energie) organization supported the work of Ms I. Manuel (Grant BOU 0050). We also thank Rhodia for purchasing the $Ce_{0.68}Zr_{0.32}O_2$ support. Finally, we thank P. Lavaud for technical support.

References

[1] R.R. Ford, Adv. Catal. 21 (1970) 51.
[2] S.E. Voltz, C.R. Morgan, D. Liederman, S.M. Jacob, Ind. Eng. Chem. Prod. Res. Dev. 12 (1973) 294.
[3] T. Engel, G. Ertl, Adv. Catal. 28 (1979) 1.
[4] G. Ertl, in: J.R. Anderson, M. Boudart (Eds.), Catalysis Science and Technology, vol. 4, Springer, Berlin, 1983, p. 238.
[5] P.J. Berlowitz, C.H.F. Peden, D.W. Goodman, J. Phys. Chem. 92 (1988) 5213.
[6] K.I. Choi, M.A. Vannice, J. Catal. 131 (1991) 1.
[7] A.K. Santra, D.W. Goodman, Electrochim. Acta 47 (2002) 3595.
[8] K.C. Taylor, in: J.R. Anderson, M. Boudart (Eds.), Catalysis Science and Technology, vol. 5, Springer, Berlin, 1984, p. 119.
[9] M. Shelef, G.W. Graham, Catal. Rev.-Sci. Eng. 36 (1994) 431.
[10] A. Cybulski, J.A. Moulijn, Catal. Rev.-Sci. Eng. 36 (1994) 179.
[11] A. Bourane, D. Bianchi, J. Catal. 209 (2002) 126.
[12] J.H.B.J. Hoebink, J.P. Huinink, G.B. Marin, Appl. Catal. A 160 (1997) 139.
[13] R.H. Nibbelke, M.A.J. Campman, J.H.B.J. Hoebink, G.B. Marin, J. Catal. 171 (1997) 358.
[14] R.H. Nibbelke, A.J.L. Nievergeld, J.H.B.J. Hoebink, G.B. Marin, Appl. Catal. B 19 (1998) 245.
[15] I. Manuel, C. Thomas, C. Bourgeois, H. Colas, N. Matthess, G. Djéga-Mariadassou, Catal. Lett. 77 (2001) 193.
[16] R. Heck, R.J. Farrauto, Appl. Catal. A 221 (2001) 443.
[17] C.H.F. Peden, D.W. Goodman, D.S. Blair, P.J. Berlowitz, G.B. Fisher, S.H. Oh, J. Phys. Chem. 92 (1988) 1563.
[18] N.W. Cant, P.C. Hicks, B.S. Lennon, J. Catal. 54 (1978) 372.
[19] S.H. Oh, C.C. Eickel, J. Catal. 128 (1991) 526.
[20] Y.F. Yu Yao, J. Catal. 87 (1984) 152.
[21] J. Kaspar, P. Fornasiero, M. Graziani, Catal. Today 50 (1999) 285.
[22] A. Trovarelli, in: G.J. Hutchings (Ed.), Catalysis by Ceria and Related Materials, Imperial College Press, London, 2002.
[23] T. Bunluesin, H. Cordatos, R.J. Gorte, J. Catal. 157 (1995) 222.
[24] S.H. Oh, C.C. Eickel, J. Catal. 112 (1988) 543.
[25] W.C. Hecker, A.T. Bell, J. Catal. 84 (1983) 200.
[26] F. Fajardie, J.-F. Tempère, J.-M. Manoli, O. Touret, G. Blanchard, G. Djéga-Mariadassou, J. Catal. 179 (1998) 469.
[27] G. Djéga-Mariadassou, F. Fajardie, J.-F. Tempère, J.-M. Manoli, O. Touret, G. Blanchard, J. Mol. Catal. A 161 (2000) 179.
[28] L. Salin, C. Potvin, J.-F. Tempère, M. Boudart, G. Djéga-Mariadassou, J.-M. Bart, Ind. Eng. Chem. Res. 37 (1998) 4531.
[29] P. Bera, K.C. Patil, V. Jayaram, G.N. Subbanna, M.S. Hegde, J. Catal. 196 (2000) 293.
[30] K.R. Priolkar, P. Bera, P.R. Sarode, M.S. Hegde, S. Emura, R. Kumashiro, N.P. Lalla, Chem. Mater. 14 (2002) 2120.
[31] C.O. Bennet, personal communication.
[32] S.H. Oh, G.B. Fisher, J.E. Carpenter, D.W. Goodman, J. Catal. 100 (1986) 360.
[33] D. Duprez, J. Chim. Phys. 92 (1995) 1952.
[34] G. Djéga-Mariadassou, M. Boudart, J. Catal. 216 (2003) 89.
[35] M. Boudart, G. Djéga-Mariadassou, Kinetics of Heterogeneous Catalytic Reactions, Princeton Univ. Press, Princeton, NJ, 1984.
[36] T.W. Root, L.D. Schmidt, G.B. Fisher, Surf. Sci. 134 (1983) 30.
[37] T. Matsushima, J. Catal. 85 (1984) 98.
[38] V.B. Goncharov, E.F. Fialko, D.E. Sheinin, A.V. Kikhtenko, Kinet. Catal. 38 (1997) 589.
[39] S. Trautmann, M. Baerns, J. Catal. 150 (1994) 335.
[40] V.P. Zhdanov, J. Pavlíček, Z. Knor, Catal. Rev.-Sci. Eng. 30 (1988) 501.
[41] R.C. Baetzold, G.A. Somorjai, J. Catal. 45 (1976) 94.
[42] O.V. Krylov, M.U. Kisliuk, B.R. Shub, A.A. Gezalov, N.D. Maksimova, Y.N. Rufov, Kinet. Catal. 13 (1972) 598.